



Anodic dissolution behavior of zirconium in Bu^n_4NBr -containing isopropanol solution

Xi-yun YANG, Hai-qiang HUANG, Sheng-hai YANG

School of Metallurgy and Environment, Central South University, Changsha 410083, China

Received 6 October 2015; accepted 23 February 2016

Abstract: Anodic dissolution behavior of zirconium in Bu^n_4NBr -containing isopropanol solution was investigated using cyclic voltammetry, linear sweep voltammetry and chronoamperometry, complemented with a scanning electron microscope (SEM). The voltammograms did not exhibit active dissolution until the breakdown of passive layer induced by aggressive bromide anions. SEM images confirmed the existence of pits on zirconium surface. The depth and breadth of pits were intensified with increasing potential. The pitting potential shifted negatively as either temperature or Bu^n_4NBr concentration was increased, while it increased with increasing scan rate. The corrosion current density increased with increasing temperature. The apparent activation energy of anodic dissolution of zirconium was 21.88 kJ/mol. The chronoamperometry revealed that increasing Bu^n_4NBr concentration shortened the incubation time for passivity breakdown and accelerated the pit nucleation and growth. The experimental results were helpful to obtain the optimum conditions for electrosynthesis of zirconium isopropoxide.

Key words: zirconium; anodic dissolution; pitting corrosion; isopropanol; tetrabutylammonium bromide

1 Introduction

Zirconium oxide has a high dielectric constant ($\epsilon=20\text{--}25$) and high refractive index. It is a promising candidate for storage capacitors in dynamic random access memories, gate oxides in field effect transistors, optical waveguides, and antireflection layers for solar cells [1–3]. Zirconium oxide is usually prepared by chemical vapor deposition of zirconium alkoxide [4,5]. Thus, zirconium alkoxide serves as an important precursor for zirconium oxide [6,7].

Electrochemical synthesis of metal alkoxide seems to be a promising method, i.e., anodic dissolution of metal in absolute alcohols in the presence of a conductive electrolyte [8], which exhibits superiority due to simplicity and high productivity as well as its continuous and non-polluting character [9]. TUREVSKAYA et al [10] synthesized niobium, zirconium and hafnium alkoxides using electrochemical method. BEREZKIN et al [11] and CAI et al [12] prepared niobium alkoxide under the same principle. YANG et al [13] prepared high-purity tantalum ethoxide by electrochemical synthesis followed by vacuum

distillation. In Russia, the electrosynthesis technique has been successfully employed for the commercial production of alkoxides of Y, Ti, Zr, Nb, Ta, Mo, W, Cu, Ge and Sn [8].

To synthesize zirconium alkoxide, it is necessary to understand the dissolution behavior of zirconium in organic solvent, notably alcohols. Zirconium is known to be a passive metal due to the presence of a protective oxide layer in aqueous solution [14]. However, its passivity is not very stable in chloride-containing solution. Chloride induced breakdown of passive film and consequently pitting occurred. The corrosion of zirconium in chloride solution has been widely investigated [15,16]. But few references describing zirconium corrosion in non-aqueous solutions have been found [17]. The corrosion behavior of titanium in non-aqueous solutions like methanol, ethanol and propanol solutions was well reported [18,19], and passivity and pitting of titanium have been investigated with respect to the effect of water and aggressive ions [20]. Zirconium and titanium are regarded as sister metals with similar physical and chemical properties such as close standard reduction potential and high affinity for oxygen. While they also show some

differences in corrosion properties in aqueous solution. For example, zirconium does not exhibit the active region as titanium and most other passive metals do at active potentials in acidic chloride solutions. Zirconium is more suitable than titanium for handling reducing acids and strong alkalis [21]. Thus, zirconium corrosion in non-aqueous solutions would be different from titanium and deserve detailed investigation.

Isopropanol is a good organic solvent due to low boiling point. It is found that Bu^n_4NBr is a good supporting electrolyte due to high conductivity and solubility in isopropanol [22]. Zirconium isopropoxide is an important precursor for zirconium oxide due to easy decomposition and hydrolysis [7]. It has high activity and acts as an important raw material for cross-linking agent in oil refinery [23]. In the present work, the electrochemical dissolution behaviors of zirconium were investigated in isopropanol solution containing supporting electrolyte Bu^n_4NBr , using cyclic voltammetry, linear sweep voltammetry and potentiostatic current–time transient techniques. The effects of applied potential, temperature, scan rate and Bu^n_4NBr concentration on the dissolution rate were discussed, which would be helpful to understand the reaction mechanism and seek the optimum synthesis conditions.

2 Experimental

2.1 Materials

The electrolyte solution was prepared using isopropanol (99.7%, Tianjing Damao), tetrabutylammonium bromide (99%, Bu^n_4NBr , Shanghai Aladdin) and acetonitrile (99%, Sinopharm Chemical Reagent Co., Ltd.). All chemicals were analytical grade and used without further purification.

Electrochemical experiments were carried out in a conventional three-electrode glass electrochemical cell. A zirconium rod (99.9% purity, 5.0 mm in diameter), purchased from Zhuzhou Cemented Carbide Group Corp. Ltd., was used as the working electrode. The apparent exposed area was 0.19 cm^2 . The counter electrode was platinum foil (about 2 cm^2). All potentials were measured and reported relative to a saturated calomel electrode (SCE). An electrolyte filled bridge with a Luggin capillary was used to minimize the IR drop.

2.2 Methods and characterization

Electrochemical measurements were performed using a potentiostat/galvanostat (CHI 660C electrochemical workstation provided by Shanghai CH Instruments, Inc.) and connected with a personal computer. Cyclic voltammetry (CV) measurements were

carried out by sweeping the potential from -1.0 V in the positive direction at a given scan rate up to the desired potential and then reversing with the same scan rate to the starting potential. Linear sweep voltammetry (LSV) experiments were conducted by changing the potential automatically from the open circuit potential to 3.7 V at a scan rate of 10 mV/s . Tafel plots were measured by changing the potential automatically from -1.0 to 1.8 V at a scan rate of 5 mV/s . The chronoamperometry (anodic current transients) at a constant anodic potential of φ_a was recorded for 20 s .

Prior to each experiment, the electrolyte solution was deaerated using ultra-pure nitrogen for 20 min and then maintained under a nitrogen atmosphere in the whole experiment. The working electrode was successively abraded with a series of emery papers, from a coarse grade 400 to fine grade 3600. After that, the electrode was rinsed with acetone, ethanol, dried and finally dipped in the electrolytic cell. The standard conditions employed were 0.08 mol/L Bu^n_4NBr , 90% isopropanol and 10% acetonitrile (volume fraction) as solvent, temperature of $(20 \pm 0.5) ^\circ\text{C}$. The addition of 10% acetonitrile was to increase the conductivity from 272 to $756 \mu\text{S/cm}$. No further drying of the solvent was carried out. The water content in the solution was 0.2% (mass fraction). Before each experiment, the electrode was allowed to corrode freely for a period of 0.5 h . After this time, a steady state open circuit potential, corresponding to the corrosion potential (φ_{corr}) of the working electrode, was obtained. The variations for these conditions are noted in the text and figure captions.

The electrode surface was examined by scanning electron microscope (SEM, model JSM–6360 LV) after anodic polarization at various potentials for 10 min in the mixed solvent containing 0.08 mol/L Bu^n_4NBr . The conductivity of electrolyte was measured using a DDS–11C conductivity meter (INESA Instrument, Shanghai).

3 Results and discussion

3.1 Effect of applied potential on zirconium dissolution

The cyclic voltammetry curve for Zr in the mixed solvent containing 0.08 mol/L Bu^n_4NBr at a scan rate of 10 mV/s is shown in Fig. 1. On the positive-going scan, the inserted plot shows a corrosion potential (φ_{corr}) of -0.72 V below which the current is cathodic. The cathodic current probably corresponds to either hydrogen evolution or reduction of residual traces of dissolved oxygen despite thorough deaeration [18,24]. The anodic current density increases from φ_{corr} to -0.3 V and then attains a plateau value about $48 \mu\text{A/cm}^2$ until 0.9 V . The low limiting current density indicates that zirconium

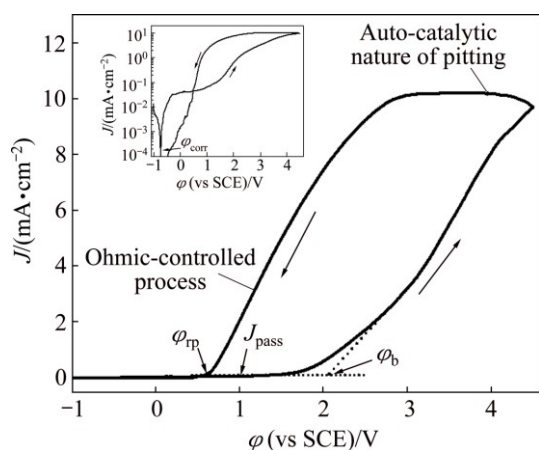


Fig. 1 Cyclic voltammograms for Zr in isopropanol with 0.08 mol/L Bu_4NBr at scan rate of 10 mV/s

does not exhibit active dissolution in the potential region from -0.3 to 0.9 V. The lack of active dissolution can be attributed to passivation due to the presence of an oxide film on zirconium surface. Such an oxide film formation should also be reflected in the change of open circuit potential with time, as shown in Fig. 2. The potential becomes more positive with time and takes about 20 min to attain a steady state. Zirconium has a remarkable capability to form zirconium oxides in an oxygen-containing environment, such as O_2 , H_2O or CO_2 . The oxide film could be formed only through contact with traces of water in the mixed solvent according to the reaction $\text{Zr} + 2\text{H}_2\text{O} = \text{ZrO}_2 + 4\text{H}^+ + 4\text{e}^-$ [21]. PALIT and ELAYAPERUMAL [17] observed that the addition of more than 1% water to methanol-anhydrous HCl solution led to stable passivity of zirconium. The critical water content needed for stable passivity is different for different cases. Titanium requires 0.12% H_2O (mole fraction) in alkaline methanolic solution, 2% H_2O (mass fraction) for *n*-propanol and 0.1% H_2O (mass fraction) for iso-propanol [19,25]. The minimum water content necessary to stabilize the oxide film decreases when the number of the carbon atoms of the aliphatic alcohol increases. It is deduced that water is involved in the oxide film formation and inhibits the dissolution of zirconium. With the potential further moving towards the positive direction, the anodic current density gradually increases, which may result from the attack of the passive film by Br^- anions [26]. When the anodic potential exceeds a certain critical value ϕ_b , the current density rises more quickly than ever before, without any sign of oxygen evolution, suggesting the breakdown of the passive film and initiation and propagation of pitting corrosion. When the potential is reversely scanned, the current density shows a continuous and small increase, typical of an autocatalytic character of pitting corrosion. Afterward, the current density begins to linearly decrease

and forms a hysteresis loop. The observed linear current–potential relationship suggests that an ohmic-controlled process takes place [27]. The existence of a hysteresis loop in a cyclic voltammetry curve indicates a delay in repassivation of an existing pit when the potential is scanned toward negative direction. The larger the hysteresis loop is, the more difficult it becomes to repassivate the pit [28]. This loop allows the repassivation potential (ϕ_{rp}) to be determined, where ϕ_{rp} corresponds to the potential values below which no pitting occurs and above which pit nucleation begins [29]. The results obtained here are in good agreement with those reported previously for Ta [30]. The locations of ϕ_{rp} and ϕ_b are well-defined in Fig. 1.

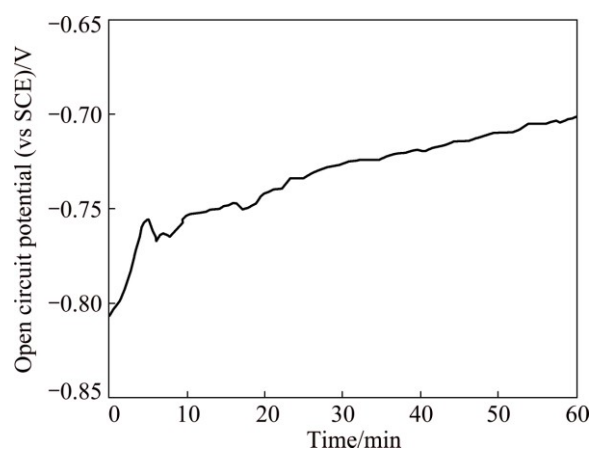


Fig. 2 Variation of open circuit potential of zirconium with time in isopropanol with 0.08 mol/L Bu_4NBr

Figure 3 shows the microscopic images of the electrode surface anodized for 10 min at various potentials. It is quite clear that the ratio of pitted area to total surface area and depth of pits vary depending on the applied potential. No pitting occurs when zirconium is held at 0.8 V (Fig. 3(a)). Anodizing at 1.8 V induces obvious pits on the specimen (Fig. 3(b)). Large and more defined pits are observed when the potential increases to 2.4 V. Further increasing potential to 3.0 V yields a rough etched surface with dense distribution of corrosion pits. The radial growth of large pits seems to begin by the coalescence of small pits. It is observed that the pits appear to be smaller and shallower than those on other eroded samples (Figs. 3(b) and (c)). The pits exhibit different breadths and depths due to nonuniformity of zirconium surface. The pit mouth is usually larger than the bottom. Thus, deep pits leave smaller and shallower cavities after the whole surface erosion and shallow pits become invisible due to the roughness of eroded surface. The increase in pitting susceptibility with an increase in potential could be explained on the basis that an increase in the applied potential may increase the electric field across the passive film and therefore enhances the

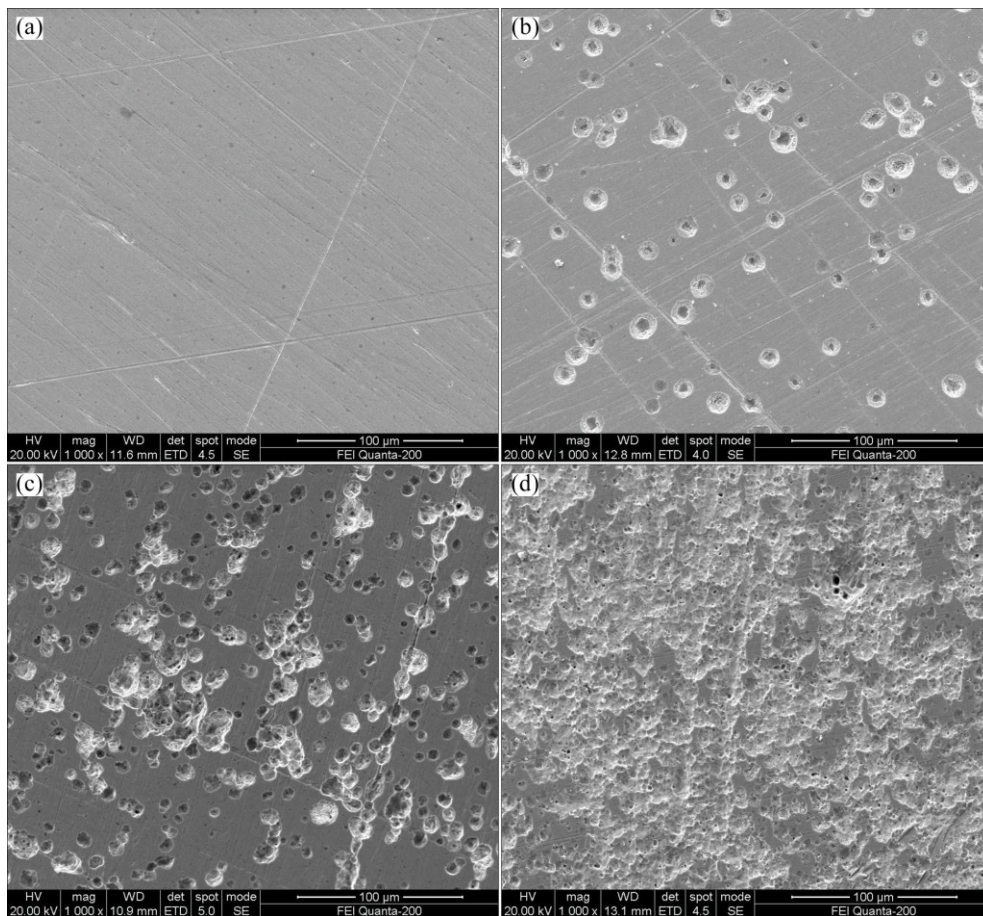


Fig. 3 Microscopic images of electrode surface anodized for 10 min at various potentials: (a) 0.8 V; (b) 1.8 V; (c) 2.4 V; (d) 3.0 V

adsorption of the aggressive Br^- anions on the passive electrode surface. Similar results are also reported by YANG et al [24] and ONO and HABAZAKI [31].

3.2 Effect of scan rate on zirconium dissolution

Figure 4 presents the effects of scan rate (ν) on the cyclic voltammetry curves of zirconium in isopropanol with 0.08 mol/L Bu_4NBr . All curves show a potential region where zirconium surface is passive at a low current density (less than $200 \mu\text{A}/\text{cm}^2$). The difference in passive current density for different scan rates is due to a balance between surface activation caused by the applied potential and passive film growth. It is obvious that ϕ_b shifts towards more positive values with an increase in scan rate. The initiation of pitting attack can be ascribed to the adsorption of Br^- anions on the passive film [24]. The adsorbed aggressive anions can penetrate through the passive layer, especially at its defect points and flaws, with the assistance of a high electric field to reach the base zirconium surface. Following this, an incubation time and a certain amount of bromide anions are needed to perforate the passive layer. At a high ν value, which corresponds to a sufficiently short incubation time, bromide ions have little time to form a soluble complex, leading to the formation of a thicker passive layer.

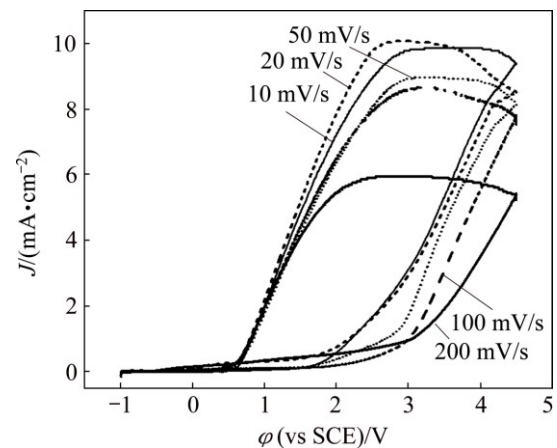


Fig. 4 Effect of scan rate (ν) on cyclic voltammetry curves of Zr in isopropanol with 0.08 mol/L Bu_4NBr

Consequently, pitting initiation occurs only at a more positive potential. It is found that ϕ_b linearly increases with an increase of $\nu^{1/2}$ (Fig. 5), a feature of pitting corrosion phenomenon.

3.3 Effect of Bu_4NBr concentration on zirconium dissolution

The effect of Bu_4NBr concentration on the linear sweep voltammetry of zirconium is given in Fig. 6. It is

observed that an increase of Bu_4NBr concentration increases the anodic current density. The acceleration effect of Bu_4NBr is due to the fact that Br^- adsorbs on zirconium surface and subsequently participates in the active dissolution to form soluble complex. Furthermore, the conductivity of electrolyte also increases with the increase of Bu_4NBr concentration, which correspondingly accelerates zirconium dissolution. For all the electrolytes, the conductivity was measured in the range from 290 to 873 $\mu\text{S}/\text{cm}$ as shown in Fig. 7. For a current density of 3 mA/cm^2 , it is estimated that the ohmic potential drop is from 47.0 to 141.5 mV [18], which becomes considerable only at high currents. Thus, the data are presented and uncorrected for IR drop. It is observed that the breakdown potential ϕ_b shifts negatively with increasing Bu_4NBr concentration. This response is interpreted that aggressive bromide anions attack the passive film and subsequently pits form. The increase of the amount of bromide ions may make passive film breakdown more easily. As a result, the initiation of pitting occurs at a more negative potential.

The current–time transients for Zr in isopropanol solution with various Bu_4NBr concentrations at a

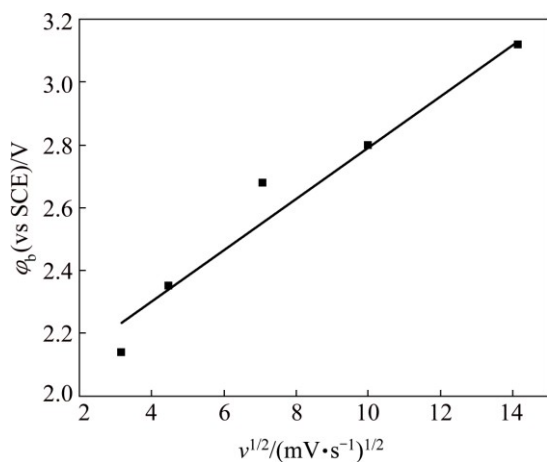


Fig. 5 Relationship between ϕ_b and $v^{1/2}$

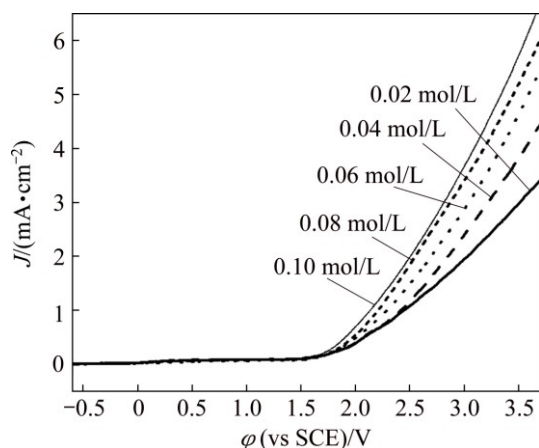


Fig. 6 Effect of Bu_4NBr concentration on linear sweep voltammetry of zirconium

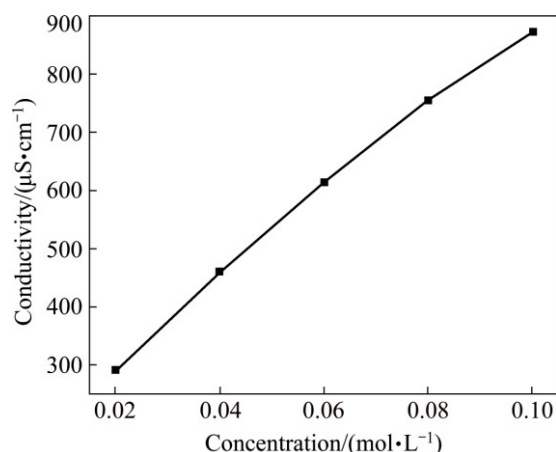


Fig. 7 Conductivity of electrolyte at different Bu_4NBr concentrations

constant anodic potential of 3.0 V are shown in Fig. 8. For all the Bu_4NBr concentrations studied, the current density initially decreases rapidly with time and reaches a minimum at a certain incubation time, t_i . The decrease in the current density is due to passive film growth on the anode surface. The reciprocal of the incubation time (t_i^{-1}) was taken as the rate of pit nucleation [30]. After t_i , the current density begins to rise and then reaches a steady state. The increase of current density is attributed to the breakdown of passivity caused by the aggressive attack of Br^- anions and subsequent formation and growth of pits. With the depth of pits developing, Br^- anions are more difficult to migrate into the pits due to the blockage of corrosion products accumulated on the anode surface. As a result, a steady-state current density is attained. With increasing Bu_4NBr concentration, t_i slightly decreases while the current density of the plateau increases. It is interpreted that Br^- anions are responsible for initiating pit formation in defect areas and enhancing the exposed metal dissolution. A higher

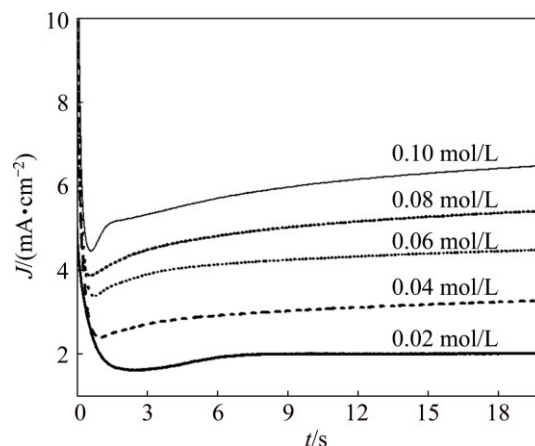


Fig. 8 Current density–time transients for Zr in isopropanol with various Bu_4NBr concentrations at constant anodic potential of 3.0 V

Br^- concentration increases the probability of initiating pit formation and accelerates pit growth. Similar results were reported for the study of pitting corrosion of different metals in several media containing aggressive anions [32,33].

To better understand the role of Br^- anions on the pit corrosion, the current density in the rising part at various concentrations of Bu_4NBr was analyzed as shown in Fig. 9. It is observed that a linear relationship between current density and $t^{1/2}$ is found and can be expressed as $J=At^{1/2}$ (where A is slope, J is current density, t is time). It is suggested that the pit growth is an instantaneous three-dimensional nucleation followed by diffusion-controlled growth and slope A could be indexed as the rate of pit growth [34]. By fitting the data, slope A can be obtained as shown in Table 1. The higher the Bu_4NBr concentrations are, the larger the values of A are, indicating that the rate of pit growth increases with an increase of Bu_4NBr concentrations.

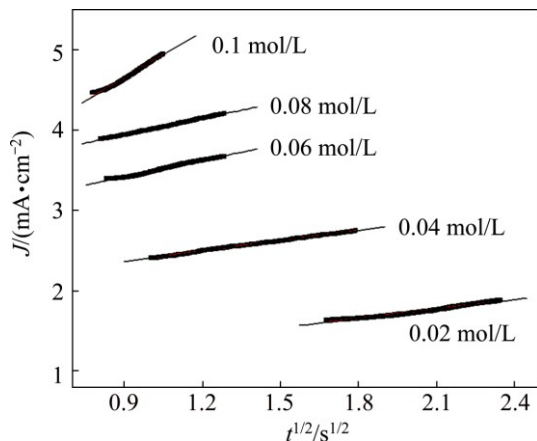


Fig. 9 Dependence of pit growth current density on $t^{1/2}$ for Zr in isopropanol with various Bu_4NBr concentrations

Table 1 Slope obtained for zirconium at various concentrations of Bu_4NBr and constant anodic potential of 3.0 V

Concentration/(mol·L ⁻¹)	0.02	0.04	0.06	0.08	0.1
Slope, $A/(\text{mA} \cdot \text{cm}^{-2} \cdot \text{s}^{-1/2})$	0.39	0.43	0.68	0.69	1.92

3.4 Effect of temperature on zirconium dissolution

The effect of temperature on the linear sweep voltammetry of zirconium is given in Fig. 10. It is shown that the anodic current density increases with increasing temperature and ϕ_b shifts towards more negative value. This behavior can be interpreted that increasing temperature enhances the solubility of passive film. This makes the thickness of the passive film decrease and its porosity increase and hence results in a less protective film. An increase in temperature also enhances the rates of diffusion and migration of the reactant and product species. Also, the adsorption of the aggressive Br^- anions is expected to increase with the increase of temperature.

All these factors accelerate pitting corrosion and stimulate anodic dissolution. As a result, ϕ_b shifts negatively and anodic current density increases with an increase in temperature.

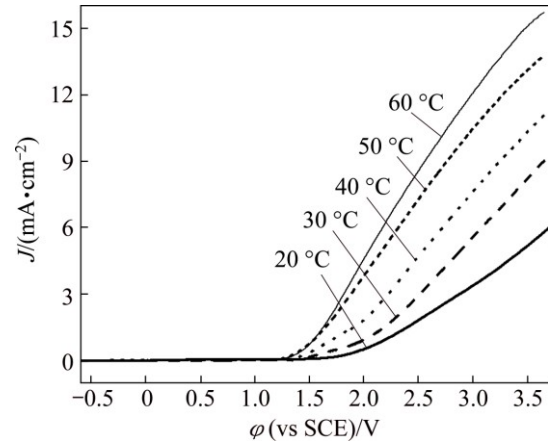


Fig. 10 Effect of temperature on linear sweep voltammetry of zirconium (0.08 mol/L Bu_4NBr , 10 mV/s)

To better understand the mechanism, Tafel plots were made at different temperatures (see Fig. 11). The corrosion current density J_c is easily calculated by extrapolating the linear logarithmic section of the anodic Tafel plots to the corrosion potential ϕ_{corr} . The current density at ϕ_{corr} is called as corrosion current density, a parameter representing the rate of corrosion. The results summarized in Table 2 show that J_c increases with increasing temperature, indicating that an increase in temperature promotes the corrosion of zirconium in isopropanol. By fixing the overpotential as 70 mV, the activation energy is simply calculated from the slope of a $\lg J$ vs $1/T$ plot shown in Fig. 12 (e.g., Arrhenius plot). The activation energy is obtained as 21.88 kJ/mol, indicative of charge transfer control for zirconium dissolution. The difference in corrosion potential can be ascribed to the change of surface state.

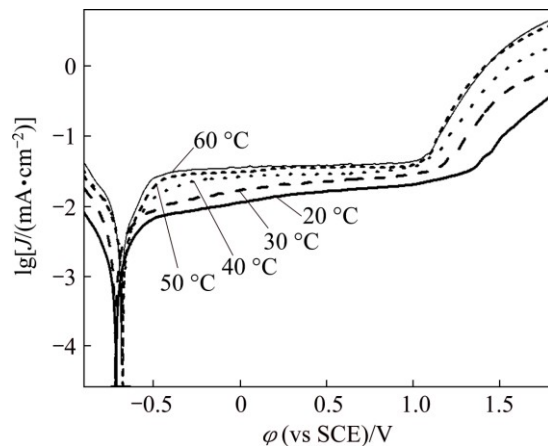


Fig. 11 Effect of temperature on Tafel plots of zirconium (0.08 mol/L Bu_4NBr , 5 mV/s)

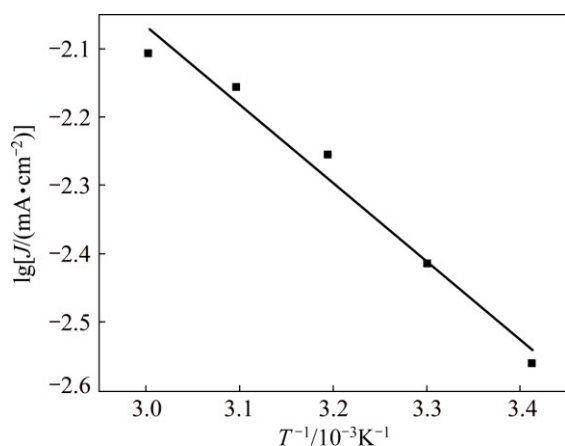


Fig. 12 Relationship between $\lg J$ and $1/T$ at overpotential of 70 mV

Table 2 Corrosion current density obtained for zirconium in isopropanol at various temperatures

Temperature/°C	20	30	40	50	60
$J_c/(\mu A \cdot cm^{-2})$	1.89	2.82	3.29	3.58	3.86

4 Conclusions

1) Zirconium does not exhibit active dissolution until the breakdown of passive layer induced by aggressive bromide anions. The dissolution conforms to pitting corrosion and forms a hysteresis loop on the CV curve. SEM images confirmed the existence of pits on the electrode surface. The depth and breadth of pits are intensified with increasing potential.

2) The pitting potential ϕ_b decreases with an increase of solution temperature and Bu^4NBr concentration, but increases with an increase of scan rate. An increase in temperature promotes the corrosion of zirconium and the apparent activation energy is 21.88 kJ/mol.

3) The potentiostatic current–time transients reveal that the anodic current density rapidly falls to a minimum value at a certain incubation time, due to the growth of a passive oxide film, then increases with the increase of time and finally attains a steady-state value. The incubation time is slightly shortened and simultaneously the steady-state current is elevated, corresponding to an increase in the rate of pit initiation and growth with increasing Bu^4NBr concentration.

4) The results inferred from this study are helpful to obtain the optimum conditions for electrosynthesis of zirconium isopropoxide as well as to get a better understanding of corrosion/passive behavior of zirconium in organic media.

References

- [1] FREIMAN G, BARBOUX P, PERRIERE J, GIANNAKOPOULOS K. Layer by layer deposition of zirconium oxide onto silicon [J]. *Thin Solid Films*, 2009, 517: 2670–2674.
- [2] DUENAS S, CASTAN H, GARCIA H, GOMEZ A, BAILON L, KUKLI K, NIINISTO J, RITALA M, LESKELA M. Electrical properties of thin zirconium and hafnium oxide high- k gate dielectrics grown by atomic layer deposition from cyclopentadienyl and ozone precursors [J]. *Journal of Vacuum Science & Technology B*, 2009, 27: 389–393.
- [3] LIU Feng, SHAN Da-yang, SONG Ying-wei, HAN En-hou. Formation process of composite plasma electrolytic oxidation coating containing zirconium oxides on AM50 magnesium alloy [J]. *Transactions of Nonferrous Metals Society of China*, 2011, 21(4): 943–948.
- [4] LIU Chun-bo, ZHANG Zhi-min, JIANG Xian-liang, LIU Min, ZHU Zhao-hui. Comparison of thermal shock behaviors between plasma-sprayed nanostructured and conventional zirconia thermal barrier coating [J]. *Transactions of Nonferrous Metals Society of China*, 2009, 19(1): 99–107.
- [5] DEZELAH C L, NIINISTO J, KUKLI K, MUNNIK F, LU J, RITALA M, LESKELA M, NIINISTO L. The atomic layer deposition of HfO_2 and ZrO_2 using advanced metallocene precursors and H_2O as the oxygen source [J]. *Chemical Vapor Deposition*, 2008, 14: 358–365.
- [6] INOUE M, KOMINAMIB H, INUI T I. Novel synthesis method for thermally stable monoclinic zirconia: Hydrolysis of zirconium alkoxides at high temperatures with a limited amount of water dissolved in inert organic solvent from the gas phase [J]. *Applied Catalysis A: General*, 1995, 121: L1–L5.
- [7] LIANG Li-ping, XU Yao, ZHANG Lei, WU Dong, SUN Yu-han, LI Zhi-hong, WU Zhong-hua. Sol-gel process of ZrO_2 and polymer doped- ZrO_2 monolayer reflective films with high laser damage threshold [J]. *Acta Physica Sinica*, 2006, 55(8): 4371–4380. (in Chinese)
- [8] BRADLEY D, MEHROTRA R, ROTHWELL I, SINGH A. Alkoxo and aryloxo derivatives of metals [M]. London: Academic Press, 2001.
- [9] SHREIDER V, TUREVSKAYA E, KOSLOVA N. Direct electrochemical synthesis of metal alkoxides [J]. *Inorganica Chimica Acta*, 1981, 53: 73–76.
- [10] TUREVSKAYA E P, KOZLOVA N I, TUROVA N Y, BELOKON A I, BERDYEYEV D V, KESSLER V G, GRISHIN Y K. The alkoxides of zirconium and hafnium: Direct electrochemical synthesis and mass-spectral study. Do “ $M(OR)_4$ ”, where $M = Zr, Hf, Sn$, really exist? [J]. *Russian Chemical Bulletin*, 1995, 44: 734–742.
- [11] BEREZKIN M Y, CHERNYKH I N, POLYAKOV E G, TOMILOV A P. Electrochemical synthesis of niobium (V) ethylate [J]. *Russian Journal of Applied Chemistry*, 2006, 79: 741–745.
- [12] CAI Ya-nan, YANG Sheng-hai, JIN Sheng-ming, YANG Hai-ping, HOU Guo-feng, XIA Jiao-yun. Electrochemical synthesis, characterization and thermal properties of niobium ethoxide [J]. *Journal of Central South University of Technology*, 2011, 18: 73–77.
- [13] YANG Sheng-hai, CHEN Yong-ming, YANG Hai-ping, LIU Yin-yuan, TANG Mo-tang, QIU Guan-zhou. Preparation of high-purity tantalum ethoxide by vacuum distillation [J]. *Transactions of Nonferrous Metals Society of China*, 2008, 18(1): 196–201.
- [14] HURLEN T, HORNKJOL S. Passive behavior of zirconium [J]. *Electrochimica Acta*, 1987, 32: 811–814.
- [15] PALIT G C, GADIYAR H S. Pitting corrosion of zirconium in

- chloride solution [J]. Corrosion, 1987, 43:140–148.
- [16] KNITTEL D R, MAGUIRE M A, BRONSON A, CHEN J S. The effect of surface treatment and electrochemical methods on the pitting potentials of zirconium in chloride solutions [J]. Corrosion, 1982, 38: 265–273.
- [17] PALIT G C, ELAYAPERUMAL K. Environment factors in stress corrosion cracking and anodic polarization of zirconium in methanol–HCl solutions [J]. Corrosion, 1976, 32: 276–282.
- [18] BURSTEIN G T, WHILLOCK G O H. The dissolution and repassivation of new titanium surfaces in alkaline methanolic solution. Part I: Phenomena [J]. Journal of Electrochemical Society, 1989, 136: 1313–1319.
- [19] WHILLOCK G O H, BURSTEIN G T. The dissolution and repassivation of new titanium surfaces in alkaline methanolic solution. Part II: The kinetics [J]. Journal of Electrochemical Society, 1989, 136: 1320–1327.
- [20] MANSFELD F. The effect of water on passivity and pitting of titanium in solutions of methanol and hydrogen chloride [J]. Journal of Electrochemical Society, 1971, 118: 1412–1415.
- [21] YAU Te-lin. Corrosion comparisons between zirconium and titanium [J]. Materials and Corrosion, 1992, 43: 358–363.
- [22] ZHOU X F, CHU A B, LIN C J. Anodic dissolution of sponge titanium in ethanol solution for preparation of nano-sized TiO_2 powder [J]. Electrochim Acta, 2002, 47: 2769–2773.
- [23] ZHUANG Yu-wei, GUO Hui, ZHANG Guo-bao, CAO Jian, WANG Ying, ZHAO Gen-suo. FTIR study of zirconium isopropoxide and zirconium *n*-butoxide decomposition in the air [J]. Spectroscopy and Spectral Analysis, 2012, 32(10): 113–114. (in Chinese)
- [24] YANG H P, YANG S H, CAI Y N, HOU G F, TANG M T. Electrochemical behavior of tantalum in anhydrous ethanol [J]. Journal of Electrochemical Society, 2010, 157(3): D168–D171.
- [25] TRASATTI S P, SIVIERI E. Electrochemical and stress corrosion cracking behavior of titanium in *n*-propanol and iso-propanol solutions [J]. Materials Chemistry and Physics, 2004, 83: 367–372.
- [26] EL-MAHDY G A, MAHMOUD S S, EIDAHAN H A. Effect of halide ions on the formation and dissolution behavior of zirconium oxide [J]. Thin Solid Films, 1996, 286: 289–294.
- [27] MUNOZ A G, BESSONE J B. Pitting of aluminum in non-aqueous chloride media [J]. Corrosion Science, 1999, 41: 1447–1463.
- [28] SZKLARSKA-SMIALOWSKA Z. Pitting corrosion of metals [M]. Houston: National Association of Corrosion Engineers, 1986.
- [29] AMIN M A, ABD EL REHIM S S, EL-LITHY A S. Pitting and pitting control of Al in gluconic acid solutions-polarization, chronoamperometry and morphological studies [J]. Corrosion Science, 2010, 52: 3099–3108.
- [30] YANG H P, YANG S H, CAI Y N, HOU G F, TANG M T. Effect of bromide ions on the corrosion behavior of tantalum in anhydrous ethanol [J]. Electrochimica Acta, 2010, 55: 2829–2834.
- [31] ONO S, HABAZAKI H. Pit growth behavior of aluminum under galvanostatic control [J]. Corrosion Science, 2011, 53: 3521–3525.
- [32] HASSAN H H, ABD EL REHIM S S, MOHAMED N F. Role of ClO_4^- in breakdown of tin passivity in NaOH solutions [J]. Corrosion Science, 2002, 44: 37–47.
- [33] REFAEY S A M, TAHA F, ABD EL-MALAK A M. Inhibition of stainless steel pitting corrosion in acidic medium by 2-mercaptobenzoxazole [J]. Applied Surface Science, 2004, 236: 175–185.
- [34] AMIN M A, ABD EL REHIM S S, EL-SHERBINI E E F. AC and DC studies of the Pitting corrosion of Al in perchlorate solutions [J]. Electrochimica Acta, 2006, 51: 4754–4764.

锆在含四丁基溴化铵异丙醇溶液中的腐蚀行为

杨喜云, 黄海强, 杨声海

中南大学 冶金与环境学院, 长沙 410083

摘 要: 采用循环伏安、线性扫描、计时电流和扫描电镜(SEM)方法研究锆在含四丁基溴化铵异丙醇溶液中的腐蚀行为。循环伏安曲线表明, 在 Br^- 击穿钝化膜诱发点蚀前, 锆在异丙醇溶液中不发生活性溶解。扫描电子显微镜证实了点蚀的发生, 且电位正移, 点蚀加剧, 深度增加, 腐蚀面积增大。随着溶液温度升高, 四丁基溴化铵的浓度增大, 锆点蚀电位均下降; 而随着扫描速度增大, 锆点蚀电位升高。腐蚀电流密度随温度升高而增大, 锆阳极溶解表观活化能为 21.88 kJ/mol 。计时电流曲线表明, 四丁基溴化铵浓度增大, 点蚀诱导时间缩短, 点蚀成核和生长速度均增大。该研究结果有利于获得电化学合成异丙醇锆的最佳工艺条件。

关键词: 锆; 阳极溶解; 点蚀; 异丙醇; 四丁基溴化铵

(Edited by Wei-ping CHEN)